JOURNAL OF MATERIALS SCIENCE 27 (1992) 5141–5148

Electron diffraction and HREM image characteristics from quasicrystalline phases in alloys of Al–Mn and Al–Mn–Si

R. PEREZ
Laboratory De Cuernavaca, Ifunam, PO Box 139-B, 62191 Cuernavaca mor., Mexico

An investigation of the quasicrystalline phases in rapidly cooled alloys of $Al_{86}Mn_{14}$ and $Al_{74}Mn_{20}Si_6$ is carried out. The Al–Mn–Si alloy shows three different kinds of phase, the icosahedral phase, the crystalline α-type phase and a third phase which resembles the decagonal T phase found in alloys of Al–Mn. Both kind of compounds (Al–Mn and Al–Mn–Si) have icosahedral diffraction patterns along similar zone axes whose lowest order diffracted vectors are different in magnitude. In the past, these extra rings of reflections were associated with the presence of superstructures. The HREM images obtained along the five-fold axis display image contrast features of similar characteristics when the specimen thickness is increased. These kind of images also show high atomic density features which are curved and modulated in intensity. These features can be seen along the five-fold, three-fold and two-fold axis. Diffraction patterns along the main icosahedral axis give rise to spots with characteristic morphology. A qualitative insight on the nature of these effects can be obtained from simulated images of density waves in a field of phasons and phonons. The Fourier transform of these images can also give a qualitative understanding of some features in the experimental diffraction patterns.

1. Introduction

During recent years a large number of investigations on the experimental and theoretical aspects of quasicrystalline materials have been carried out [1]. On the experimental side, there are currently a large number of alloys which, under different composition and cooling rates, give rise to quasicrystalline phases with very different characteristics such as icosahedral phases, decagonal and dodecagonal [2]. Furthermore, there is already experimental evidence of the presence of defects and antiphase boundaries in these type of materials. It is important to mention that conventional transmission electron microscopy of these types of structures display image contrast characteristics with strong similarities to those obtained in crystalline specimens, thus, for example, thickness fringes contours, stacking fault type of fringes, dislocation type of intensity variations have recently been reported [3–6]. HREM images, on the other hand, have also been widely reported [7]. On the theoretical side, however, very few electron microscope image simulations based on the dynamical theory of electron diffraction have been carried out [8]. One of the main reasons for little attention being paid to this topic is related with the lack, up to the present, of an appropriate atomic structural model for the quasicrystalline phases. Recent experimental results [9, 10], on the other hand, have shown that the α-cubic phase of an Al–Mn–Si alloy could be used as a first approximation to the icosahedral phase in the same alloy. There is experimental evidence which suggests the same kind of local atomic environment for both types of structures [9, 10]. Furthermore, a possible atomic structural model has already been suggested for the icosahedral phase based on the α-cubic structure [11]. The icosahedral phase in this type of alloy is, therefore, one of the few candidates which could be used in comparison between experimental electron microscope images and theoretical simulations based on the dynamical theory of electron diffraction. It is in this context that a more complete electron microscope investigation in this type of quasicrystalline phase should be carried out. The work presented in this communication explores, therefore, some of the properties and image contrast characteristics of these types of phase. Particular attention is paid to the icosahedral phases and some qualitative insights are made on the relationships between image contrast behaviour, diffraction patterns characteristics and structure.

2. Experimental procedure

The specimens have been prepared using two popular rapid solidification techniques. For the Al–Mn–Si case, a splat-cooling machine has been used. In this case the samples were prepared in an Ar gas atmosphere and the resulting "splat" was of the order of 50 μm thick and 20 mm in diameter. The original alloy-sphere to be splated was approximately 3 mm in diameter. The solidification rates obtained with this

0022–2461

process are in the range of 10^6 K s^{-1} [12]. The Al–Mn specimens were, however, obtained in a melt spinning machine. Ribbons of approximately 3 mm wide and 200 μm in thickness were produced. For electron microscope observations, the samples have been thinned using an Ar ion beam milling machine. The observations were carried out in a JEOL-2000C.

3. Experimental results

The morphology of the alloys is characterized by the presence of different phases. In the Al–Mn case, as has been commonly reported, the icosahedral phase is found surrounded by an Al matrix [13]. The sizes of the icosahedral domains are commonly in the order of a few hundred nanometres. In this alloy, however, there were no signs of the presence of the decagonal T phase. In the Al–Mn–Si alloy, three main phases can be found. The crystalline phase commonly known in these alloys as the α-phase has been obtained and also the icosahedral phase, which in this alloy displays different grain sizes. These sizes range from very small quasicrystalline domains (~ 10 nm) up to the usual domain size (~ 1 μm). The third phase found in this compound has some characteristics which are similar to the decagonal phase found in Al–Mn alloys, the so-called T phase [13, 14]. It is interesting to mention that in the past the T phase has been obtained under slower cooling rates. In this case the Al–Mn–Si alloy has been prepared under very fast cooling rates (10^6 K s^{-1}).

3.1. Structural characteristics of the phases found in the Al–Mn–Si alloy

The structural relationships between the icosahedral phases and the decagonal T phase in the Al–Mn alloy have been widely studied in the past [13, 14]. The T phase has been found to be formed when the solidification velocity decreases. It has also been reported the coexistence between both phases (T and icosahedral phases) and the epitaxial growth of the T phase on the icosahedral phase surface. One of the phases found in the Al–Mn–Si alloy resembles some of the diffraction patterns of the T phase obtained in Al–Mn. This is illustrated in Fig. 1. Fig. 1a shows a BF image of this type of phase. The characteristic striated image contrast, which has been identified in the past as one of the fingerprints of the T phase in Al–Mn [13] can clearly be seen. Fig. 1b to f shows, on the other hand, some of the more common diffraction patterns which correspond to this phase. Similar diffraction patterns have already been reported in the literature for the T phase in Al–Mn alloy [15]. The coexistence between the icosahedral phase of Al–Mn–Si and the phase with some characteristics similar to the decagonal T phase is illustrated in Figs 2 and 3. Fig. 2a shows a BF image of both phases and Fig. 2b and c their respective diffraction patterns. In this case the icosahedral grain is oriented close to a five-fold zone axis and the adjacent phase is, however, oriented along a two-fold axis. Under these diffraction conditions the interphase is not sharp as has been previously reported for the Al–Mn case [13]. The boundary region is approximately between 10 and 20 nm wide. Another type of coexistence is characterized by both phases being oriented along the same quasicrystalline zone axis. This is illustrated in Fig. 3 where the icosahedral grain and the adjacent phases are both oriented along the three-fold axis. Under these diffraction conditions the interphase is not well defined, suggesting a continuous kind of transformation from the icosahedral to the faulted phase.

3.2. Diffraction patterns morphological characteristics

Some of the diffraction patterns obtained along the icosahedral zone axis in both Al–Mn–Si and Al–Mn alloys display particular morphological characteristics. In some cases elongated spots can clearly be seen. This is illustrated in Fig. 4a, b and c obtained from the icosahedral phase in the Al–Mn–Si alloy. Elongated spots on the five-fold, three-fold and two-fold diffraction patterns can be easily identified. Furthermore, some particular spot shapes can also be found, thus, for example, triangular shapes are commonly obtained in the Al–Mn icosahedral phase. This is shown in Fig. 5, where a five- and a three-fold diffraction pattern obtained from this phase show reflections which have a pronounced triangular shape. Another characteristic of the reflections in these types of diffraction pattern are related with the asymmetry frequently observed in the overall intensity distribution on the spots. In some cases subsidiary intensity maxima can be seen. This is illustrated in Fig. 6, where some reflections have an asymmetric distribution of intensity. One aspect of interest in these icosahedral diffraction patterns is the presence of superstructure reflections. As has been previously reported [16], the icosahedral phase of Al–Mn–Si has diffraction patterns with extra inner rings of reflections associated with the presence of superstructures in the phases. This is illustrated in Fig. 7 where diffraction patterns along some of the main icosahedral zone axis display this particular kind of behaviour. It is, however, interesting to point out that the same kind of property in the diffraction patterns can also be obtained in the icosahedral phase of Al–Mn. Fig. 8 shows five-fold diffraction patterns from the Al–Mn alloy where this property can clearly be seen.

3.3. Image contrast features in HREM images

HREM images of quasicrystalline structures obtained along the main icosahedral zone axis have been widely studied in the past [7]. The lack of an appropriate atomic structural model has, however, generated few attempts to theoretically simulate these type of HREM images [8]. Mainly qualitative comparisons between image contrast characteristics and theoretical predictions have, therefore, been carried out [17]. One of the main image contrast features pointed out in the literature is related with the strong modulation in intensity that some high atomic density rows in these

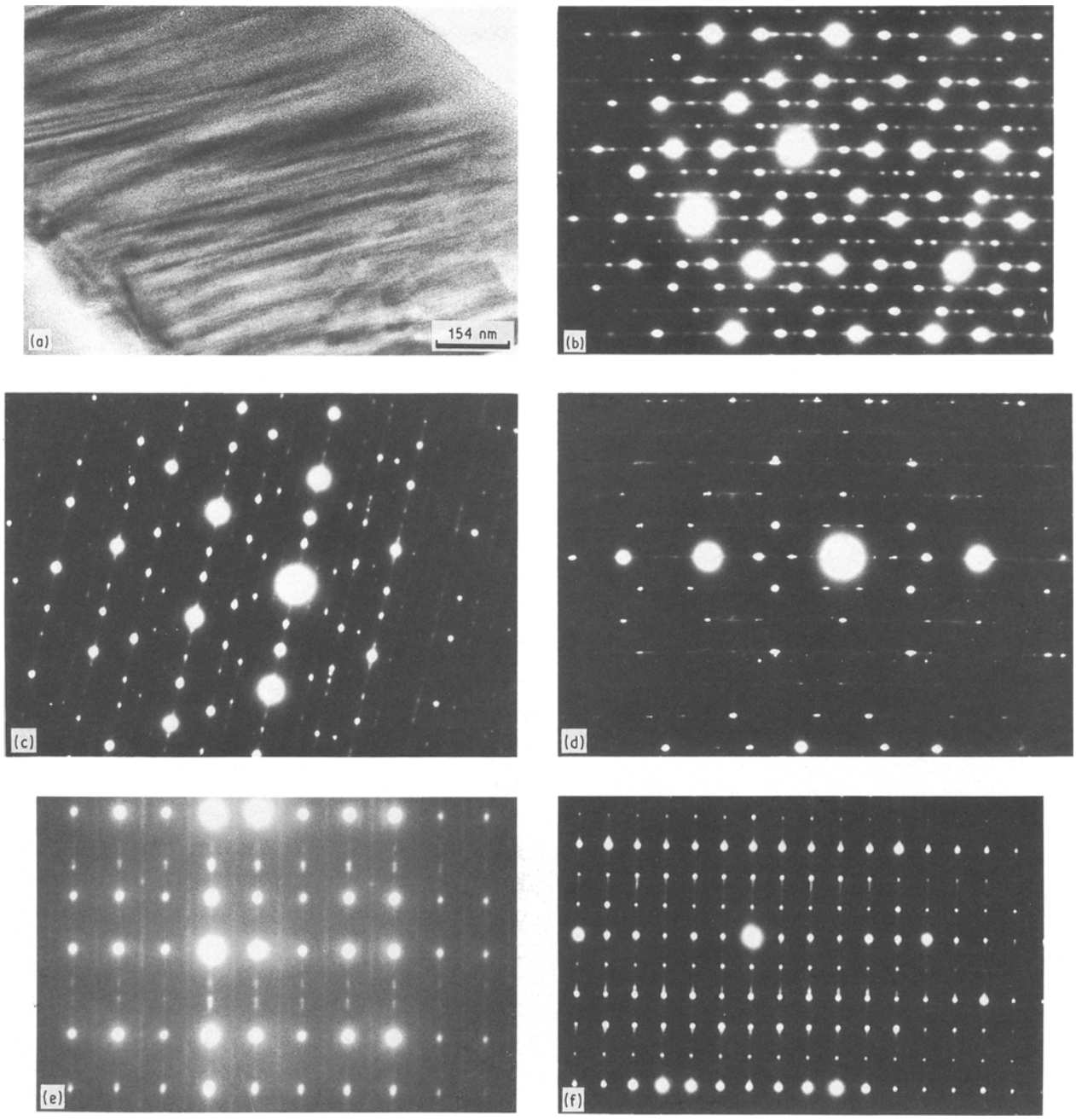

Figure 1 (a) BF image of a phase of Al–Mn–Si which resembles the T phase in Al–Mn. (b)-(f) Common diffraction patterns from this phase along different zone axis.

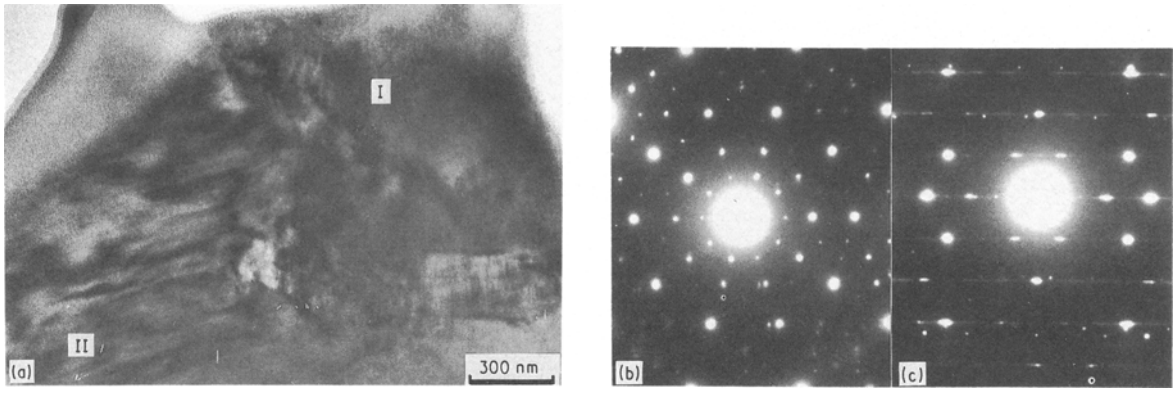

Figure 2 (a) BF image of the coexistence between the icosahedral phase and the other phase where some diffraction patterns resemble the T phase (I icosahedral; II the other phase). (b), (c) Their respective diffraction patterns, the icosahedral phase along a five-fold zone axis and the adjacent phase along a two-fold axis.

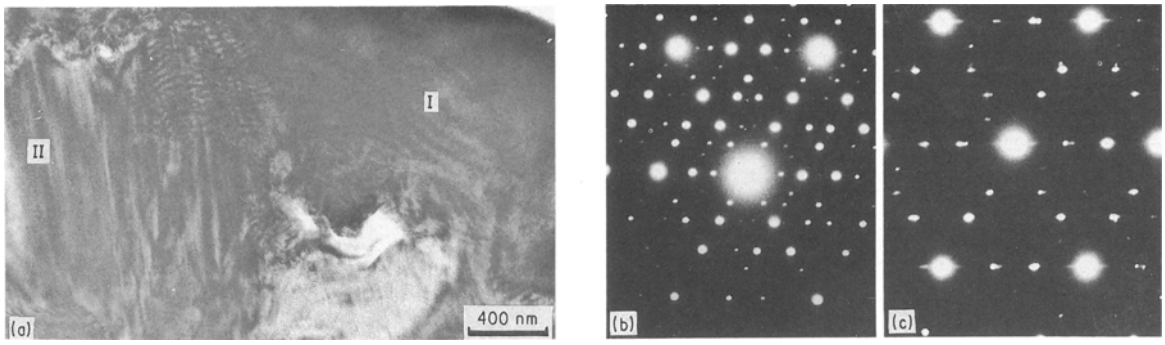

Figure 3 (a) BF image of the coexistence between the icosahedral phase and the phase which resembles the T phase (I icosahedral; II the other phase). Both phases are oriented along the same quasicrystalline zone axis. (b), (c) Their respective diffraction patterns.

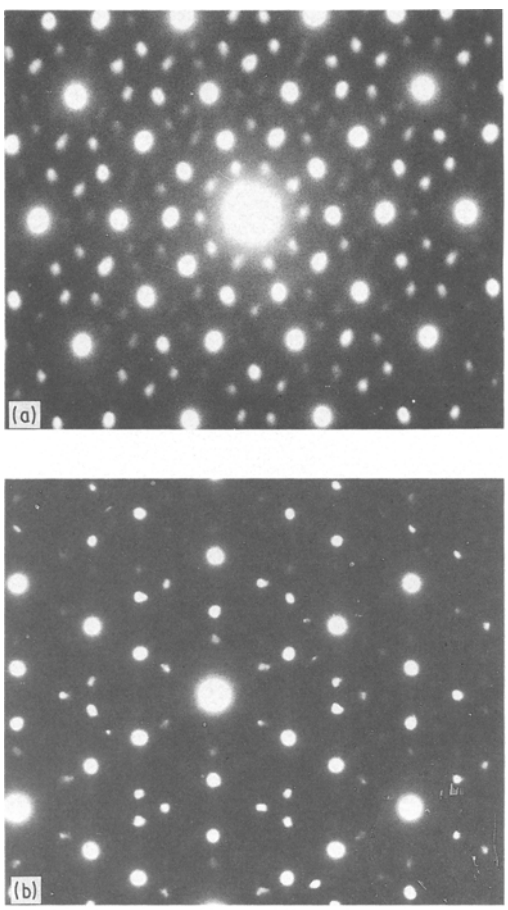

Figure 4 Diffraction patterns along (a) the five-fold, (b) the three-fold and (c) the two-fold zone axis. All the diffraction patterns show pronounced elongated spots.

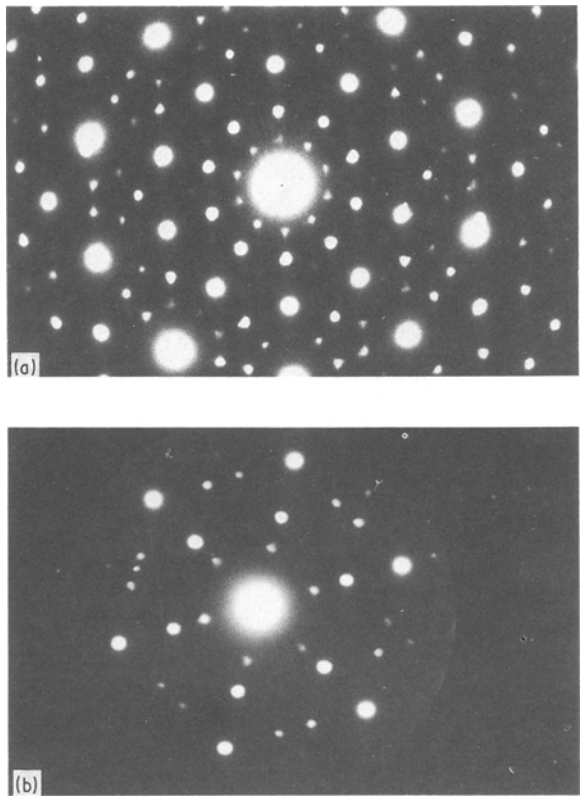

Figure 5 (a) Five- and (b) three-fold diffraction patterns from the icosahedral phase of Al–Mn. Triangular shape reflections can clearly be seen.

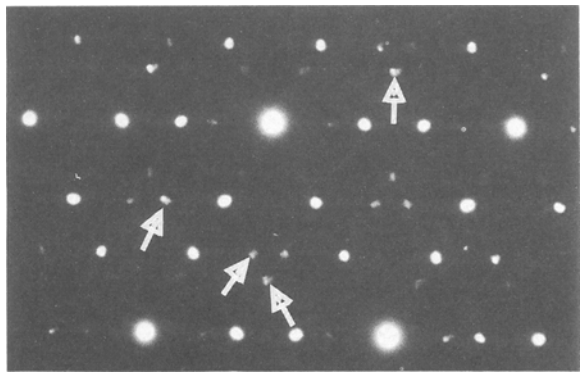

Figure 6 Reflections from a three-fold icosahedral diffraction pattern which show appreciable asymmetry distribution of electron intensity.

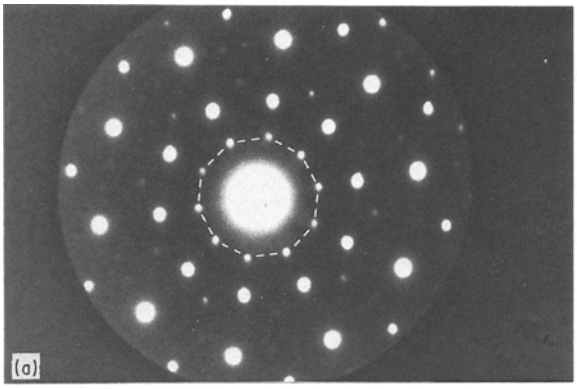

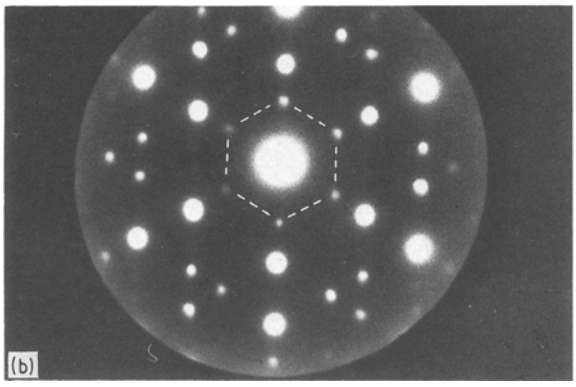

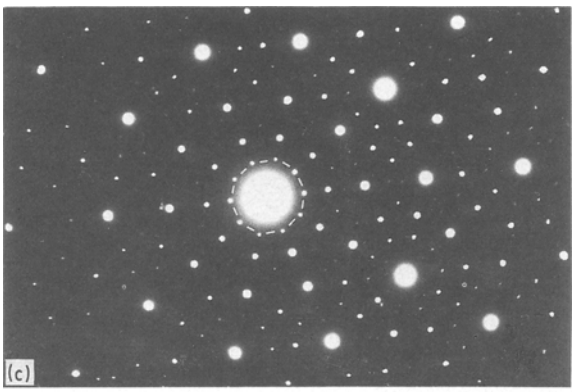

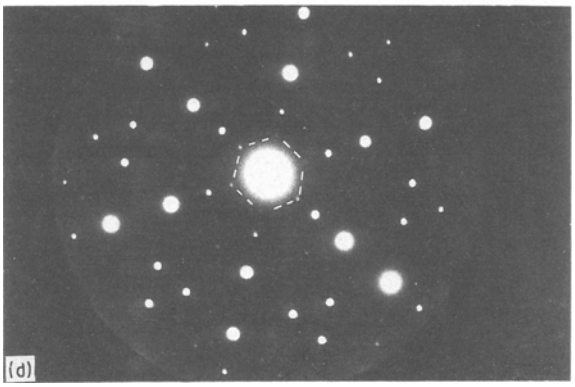

Figure 7 Diffraction patterns along the five-fold and the three-fold zone axis from Al–Mn–Si. (a), (b) Normal diffraction patterns. (c), (d) An inner extra ring of reflections can be seen along the five-fold and three-fold zone axis.

types of HREM images can commonly be seen. This is illustrated in Fig. 9 where HREM images along the five-fold, three-fold and two-fold from the icosahedral phase of Al–Mn–Si are shown. The strong modulations in the atomic rows can clearly be seen along particular directions (Fig. 9a) in the images obtained

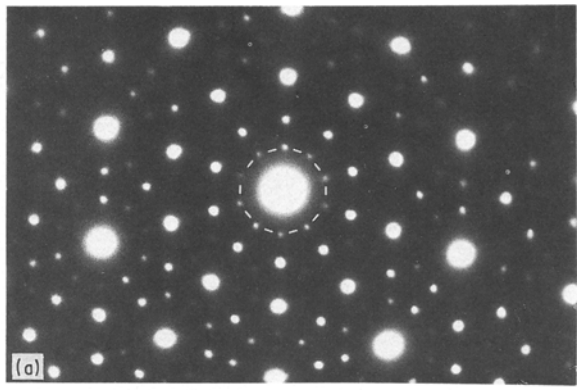

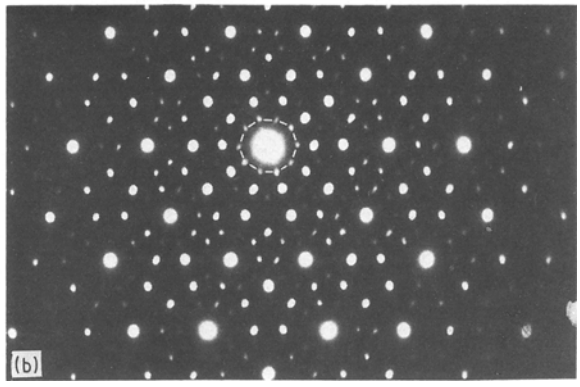

Figure 8 Five-fold diffraction patterns from Al–Mn. (a) Normal diffraction pattern. (b) Extra inner ring of reflections.

along the five-fold axis. The images obtained from the same specimen along the three-fold and the two-fold axis do not, however, indicate this type of image contrast behaviour (Fig. 9b and c). It is interesting, on the other hand, to point out that some HREM images along the two-fold and three-fold axis show in particular cases the curved rows of modulations in intensity (Fig. 10a and b).

Another interesting feature commonly found in HREM images obtained along the five-fold axis is illustrated in Fig. 11. Similar image contrast features regions can clearly be seen from this figure. The dimensions of these features are related in dimensions approximately through the constant $\tau = 1.61$ and increases in size as the thickness of the specimen is increased.

4. Discussion

Various theoretical approaches have been discussed in the literature for the qualitative analysis of the quasi-crystalline structures [17–20]. An approach which closely resembles some of the image contrast features obtained in HREM images of icosahedral phases is based on the density wave technique [17]. Density wave images can also resemble the image contrast features obtained in scanning tunnelling images of the icosahedral phase along the five-fold axis [21].

In a density wave description the mass density $\rho(\boldsymbol{r})$ is expanded in a Fourier series

$$\rho(\boldsymbol{r}) = \sum_{g \in L_R} \rho_g \exp(i\boldsymbol{g}\cdot\boldsymbol{r})$$

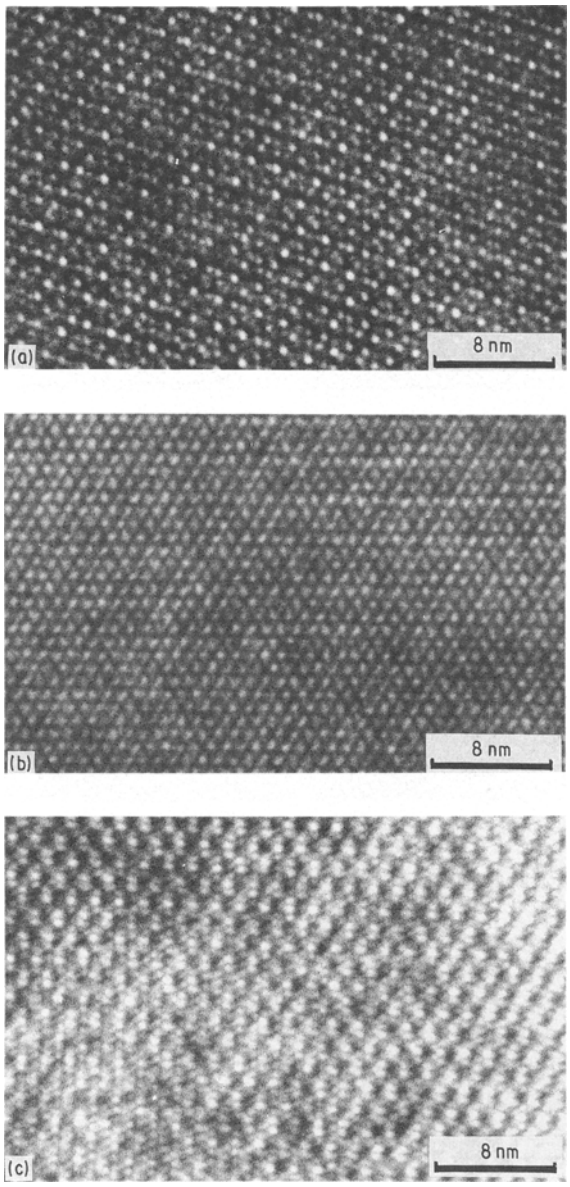

Figure 9 HREM images of Al–Mn–Si. (a) Along the five-fold axis. Strong modulations along high intensity rows can be seen. Some rows have appreciable curvature. (b) Along the three-fold axis and (c) Along the two-fold axis.

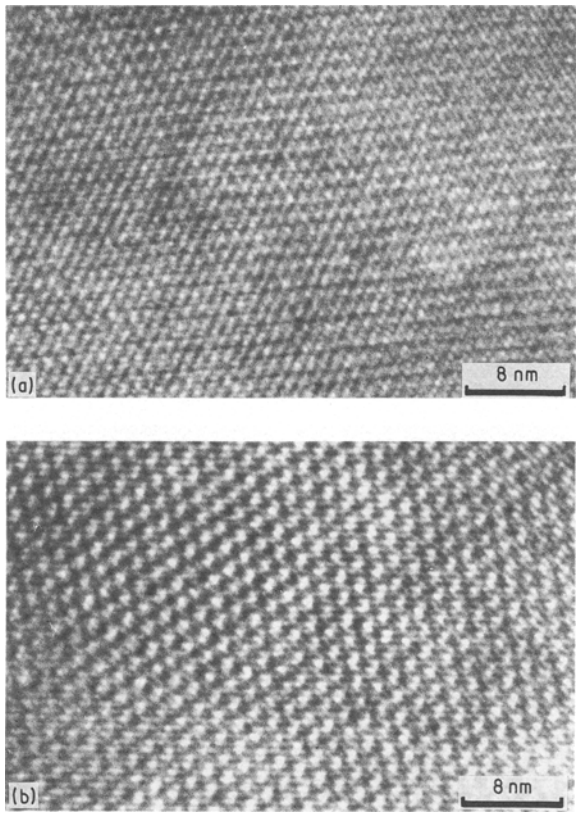

Figure 10 (a) HREM image obtained along the three-fold. Strong modulations can be seen. (b) HREM image along the two-fold axis. Some of the high intensity rows are curved.

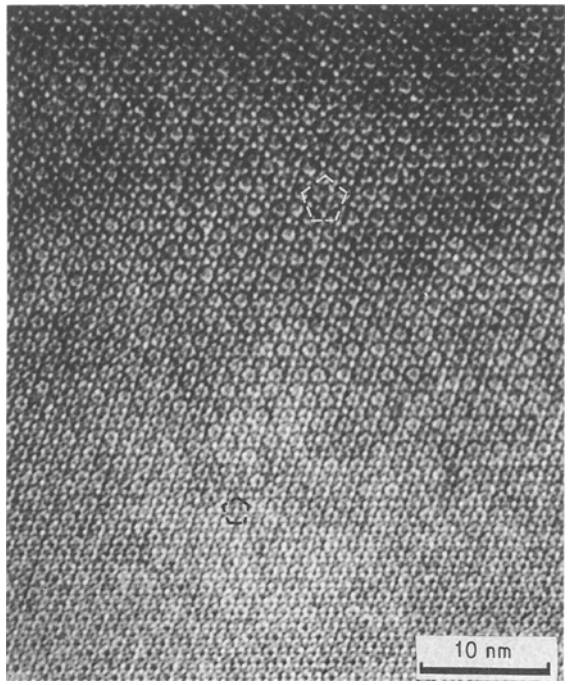

Figure 11 HREM image obtained along the five-fold zone axis. Similar image contrast features regions can clearly be seen.

where $\boldsymbol{g}$ is a reciprocal vector and L_R is the reciprocal lattice. Each ρ_g is a complex number with an amplitude ρ_g and a phase ϕ_g. For pentagonal type of structures a choice for ρ_g consists of the five vectors that point to the vertices of a pentagon. ϕ_{g_n} in this case can be written as

$$\phi_{g_n} = \boldsymbol{u}\cdot\boldsymbol{g}_n + a\boldsymbol{w}\cdot\boldsymbol{g}_{3n}$$

where spatial variations in $\boldsymbol{u}$ give rise to propagating phonons and the $\boldsymbol{w}$ variable is close related with phasons firstly defined in incommensurate crystals [17]. Calculations based on this approach are illustrated in Fig. 12. Fig. 12a shows a density wave image obtained by summing five pentagonally oriented density waves where $\sum\phi_{g_n} = 0$. Fig. 12b shows the same kind of image as in Fig. 12a, however, a dot is placed at all points $\boldsymbol{r}$ where $\rho(\boldsymbol{r})$ exceeds 70% of the maximum value. From this figure straight high density rows can clearly be seen. Fig. 12c shows the calculated Fourier transform obtained from Fig. 12a. Ten spots associated with the five-vectors used to generate the image are shown. Fig. 13, on the other hand, shows the case where a spatial variation of $\boldsymbol{u}$ and $\boldsymbol{w}$ is taken into account. In contrast to Fig. 12, the high density regions remain along rows but the rows are sometimes

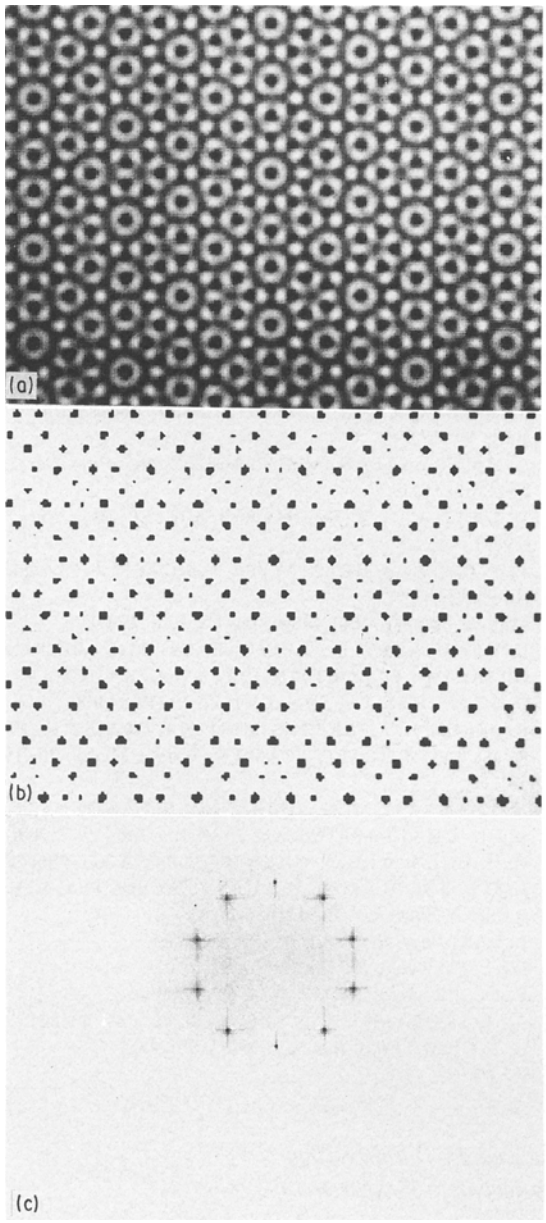

Figure 12 (a) A perfect pattern ($\sum \phi_{g_n} = 0$) obtained by summing five pentagonally oriented density waves. (b) As (a) but high intensity values are displayed. (c) Fourier spectrum obtained from (a).

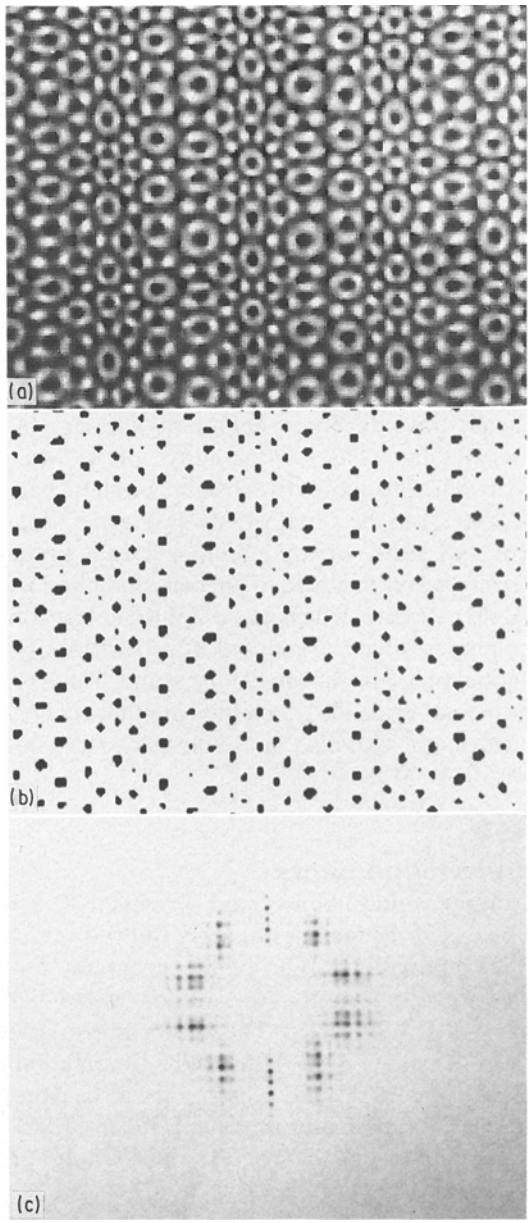

Figure 13 (a) Density wave image assuming a sinusoidal spatial variation of u and w. Shifted and curved high-density rows can be seen. (b) As (a) but only high intensity values are displayed. (c) Spectrum obtained from (a). Deformed reflections can be clearly seen.

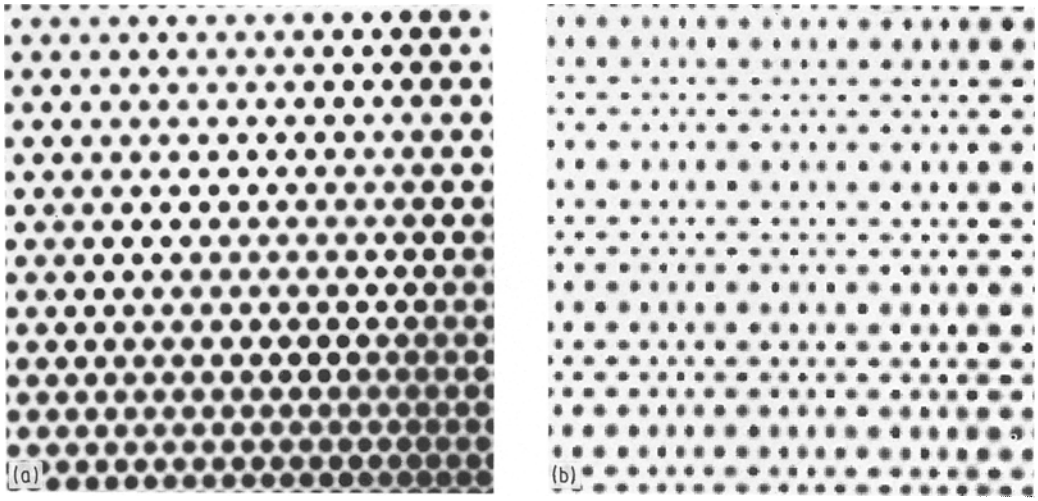

Figure 14 (a) Perfect pattern ($\sum \phi_{g_n} = 0$) of density waves along a three-fold axis. (b) Density wave image along the three-fold axis with spatial variation in u.

shifted and in some regions pronounced curvature can be seen. The calculated spectrum, on the other hand shows deformed spots with subsidiary maxima. Interestingly, some experimental micrographs shown in Section 3 resemble these image contrast features. The same kind of behaviour can also be obtained for density wave images along other icosahedral zone axes. This is illustrated in Fig. 14 where a three-fold density image is displayed.

5. Conclusions

The results presented in this communication show HREM image features and electron diffraction characteristics which are commonly present in the quasicrystalline phases from alloys of Al–Mn and Al–Mn–Si. Some qualitative insights on these particular features can be obtained by just generating the images and their corresponding spectrum produced by density waves in a field of phasons and phonons. In the Al–Mn–Si case, which was obtained at fast cooling rates, phases which are closed approximants to the decagonal phase in Al–Mn can be found. There is also experimental evidence which indicate that superstructure reflections can also be found in quasicrystalline phases of Al–Mn.

Acknowledgements

The author would like to thank Professor K. Urban who provided the facilities to carry out this investigation. For providing some of the programs for the density wave calculation the author would like to thank Mr M. Wollgarten. The author is also grateful to the Alexander Von Humboldt Foundation for financial support. Finally, thanks are also expressed to the KFA Forschungszentrum, Julich, FRG for allowing me to work there a year and CONACYT for financial support through project 0048E.

References

1. P. J. STEINHARDT and S. OSTLUND, "The Physics of Quasicrystals" (World Scientific, Singapore, 1987).
2. CH. JANOT and J. M. DUBOIS, *J. Phys. F.* **18** (1988) 2303.
3. Y. CALVAYRAC, J. DEVAUD-RZEPSKI, M. BESSIERE, S. LEFEBVRE, A. QUIVY and D. GRATIAS, *Phil. Mag. B* **59** (1989) 439.
4. J. DEVAUD-RZEPSKI, A. QUIVY, Y. CLAVAYRAC, M. CORNIER-QUIQUANDON and D. GRATIAS, *Phil. Mag. B.* **61** (1990) 286.
5. Z. ZHANG and K. URBAN, *Phil. Mag. Lett.* **60** (1989) 97.
6. J. REYES-GASGA, J. G. PEREZ-RAMIREZ and R. PEREZ, *J. Mater. Res.* **3** (1988) 29.
7. K. HIRAGA, M. HIRABAYASHI, A. INOVE and T. MASUMOTO, *Sci. Rep. Inst. Tohoku Univ.* **A32** (1985) 309.
8. M. CORNIER-QUIQUANDON, PhD Thesis, University Paris VI (1988).
9. Y. MA, E. A. STERN and C. E. BOULDING, *Phys. Rev. Lett.* **57** (1986) 1611.
10. D. GRATIAS, J. W. CAHN and B. MOZER, *Phys. Rev. B* **38** (1988) 1643.
11. J. W. CAHN, D. GRATIAS and B. MOZER, *J. Physique* **49** (1988) 1225.
12. Manual Splat-Cooling Steverung Fa. Eifa (1985).
13. L. BENDERSKY, R. J. SCHAEFER, F. S. BIANCANIELLO, W. T. BOETTINGER, M. J. KAUFMAN and D. SCHECHTMAN, *Scripta Metall.* **19** (1985) 909.
14. R. PEREZ, J. G. PEREZ-RAMIREZ, A. GOMEZ, R. HERRERA and M. JOSE-YACAMAN, *Scripta Metall.* **20** (1986) 401.
15. N. THAGARAJ, G. N. SUBBANNA, S. RANGANATHAN and K. CHATTOPADHYAY, *J. Micros.* **146** (1987) 287.
16. C. H. CHEN and H. S. CHEN, *Phys. Rev. B* **33** (1986) 2814.
17. J. E. S. SOCOLAR, T. C. LUBENSKY and P. J. STEINHARDT, *Phys. Rev. B* **34** (1986) 3345.
18. P. BAK, *Phys. Rev. Lett.* **54** (1985) 1517.
19. *Idem., Phys. Rev. B* **32** (1985) 5764.
20. V. ELSER, *Acta Crystallogr. A* **42** (1986) 36.
21. A. R. KORTAN, R. S. BECKER, F. A. THIEL and H. S. CHEN, *Phys. Rev. Lett.* **64** (1990) 200.

Received 23 October 1990
and accepted 25 March 1991